Geometric factors affecting I-section struts experiencing local and strong-axis global buckling mode interaction

Elizabeth L. Liu, M. Ahmer Wadee*

Department of Civil and Environmental Engineering, Imperial College London, South Kensington Campus, London SW7 2AZ, UK

Abstract

A recent analytical model describing the post-buckling behaviour of an I-section strut experiencing strong axis global–local buckling interaction is extended to investigate the effects of modifying the strut geometry. Using a combination of analytical and finite element (FE) methods, the global and local slendernesses are varied parametrically, in turn, to determine the geometries leading to regions of interactive behaviour. The effect of stress relieved initial global imperfections are also investigated. It is observed that the strut can exhibit one of five distinct post-buckling behaviours, the geometries for which are identified. The strut can exhibit global buckling only, local buckling only, global–local buckling interaction with either the global or local mode being triggered first or the most severe case where both global and local buckling modes are triggered simultaneously. The strut is found to be highly sensitive to initial imperfections in the interactive region; the implications for imperfection sensitivity on the design and the practical use of such components are discussed.

Keywords: Analytical modelling; Mode interaction; Nonlinear mechanics; Strong axis global buckling

1. Introduction

The use of thin-walled structural steel components is widespread in the engineering industry and is popular due to their advantageous load capacity to self-weight ratios. However, thin-walled components are often prone to complex failure mechanisms that can have potentially dangerous consequences [1, 2, 3, 4]. Geometric effects and initial imperfections can also have a large impact on the behaviour of thin-walled components due to their relative vulnerability to structural instability [5, 6, 7, 8, 9, 10, 11, 12]. In the authors' previous work, an analytical model describing the interactive post-buckling behaviour of an I-section strut under compression is formulated [13, 14]. The strut buckles

*Corresponding author

Email addresses: elizabeth.liu07@imperial.ac.uk (Elizabeth L. Liu), a.wadee@imperial.ac.uk (M. Ahmer Wadee)

globally about the strong axis of bending, interacting with local buckling in both the flange and web. In the current paper, the previously formulated analytical model is summarized and subsequently exploited to analyse the effects of modifying the geometry of the I-section strut. In a similar study on an idealized strut by van der Neut [5], it was found that the post-buckling behaviour of the strut may be neutral, stable or unstable depending on the geometric properties, as shown in Fig. 1, and it is anticipated that a similar response will

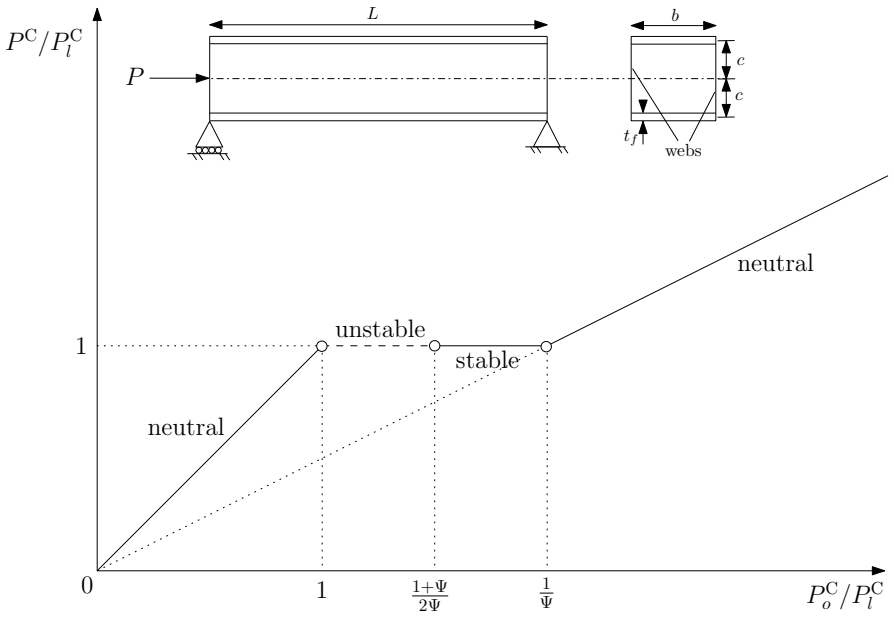


Figure 1: The van der Neut graph [5] for the post-buckling response of a strut with two load bearing flanges of width b and length L. The quantity Ψ is a stiffness reduction factor and P is the applied compression load with P^{C}, P_o^{C} and P_l^{C} being the critical, global and local buckling loads respectively. The webs of height $2c$ are idealized as rigid since the flange separation is invariant along the length with no longitudinal stiffness.

be observed presently while varying the geometric properties of the I-section strut.

A series of parametric studies is conducted to investigate the effects of modifying the global slenderness first by varying the length of the strut, and subsequently the local slenderness of the web by varying the cross-section height. A combination of analytical and finite element (FE) methods are used. Initially, the perfect, elastic strut is considered with no material or geometric imperfections. The effect of an initial global out-of-straightness imperfection is subsequently investigated.

It is found that there are four distinct regions of post-buckling behaviour that can be identified for both cases where the strut length or the cross-section height is changed. For the case where the global buckling load is much greater than the local buckling load, *i.e.* for stocky columns or deep cross-sections, local buckling is dominant and the post-buckling behaviour of the strut is stable. Conversely, when the global buckling load is much smaller

than the local buckling load, *i.e.* for long columns or shallow cross-sections, global buckling is dominant and the post-buckling behaviour is approximately neutral. An interactive region can be identified between these two bounds, where strong axis global–local mode interaction is observed. This region can be further sub-divided into one part where the local buckling mode is critical and a second part where the global buckling mode is critical. The different characteristics of each region are examined in detail and subsequently discussed. Moreover, the potential effects of plasticity are discussed by identifying when first yield would occur. This adds a more practical dimension to the current study by identifying the limiting slendernesses where plasticity effects take hold.

2. Analytical model

The elevation and cross-section of the strut under consideration, along with the notation used, are shown in Fig. 2. The strut is constructed from a linear elastic, homogeneous and

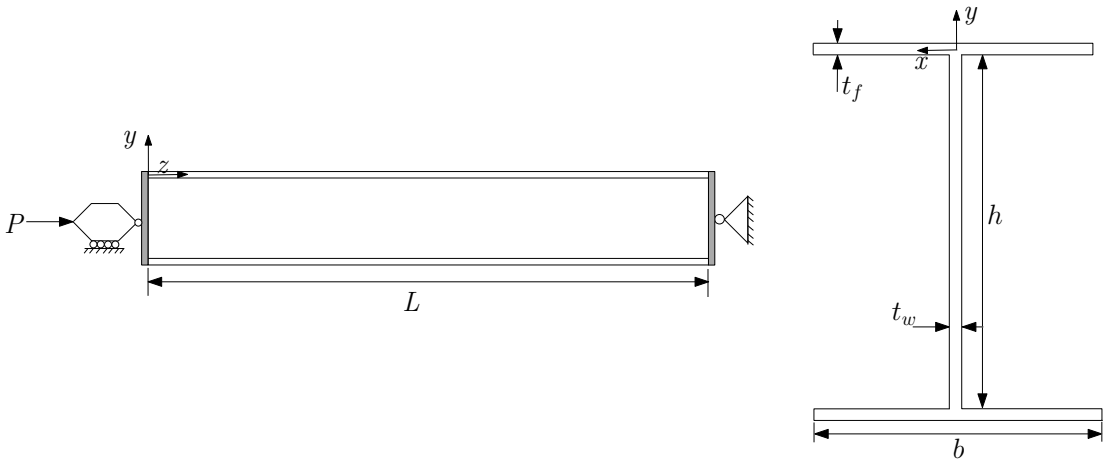


Figure 2: An I-section strut under axial loading P, elevation (left) and cross-section (right) shown. The notation and coordinate system used throughout are shown.

isotropic material and it is assumed that the strut is prevented from buckling about the weaker y-axis, a practice often used in design to increase the load carrying capacity of structural components, thereby increasing its economy. The strut is therefore forced to buckle globally about the x-axis and the load is applied concentrically as shown. Long struts are primarily considered for the analytical model; it is assumed, therefore, that global buckling is critical.

2.1. Buckling modes

The analytical model begins by defining the functions used to describe the global and local buckling shapes, as detailed in [14]. The global mode is decomposed into two components such that shear strains can be taken into account; $W(z)$ for the 'sway' and $\theta(z)$ for the

'tilt', with magnitudes of q_s and q_t defining their respective amplitudes. Additionally, the displacements $W_0(z)$ and $\theta_0(z)$ are also defined to represent their respective stress-relieved global initial imperfections, with initial displacements q_{s0} and q_{t0}. The global buckling modes, along with the respective imperfections, are shown in Fig. 3 and the corresponding

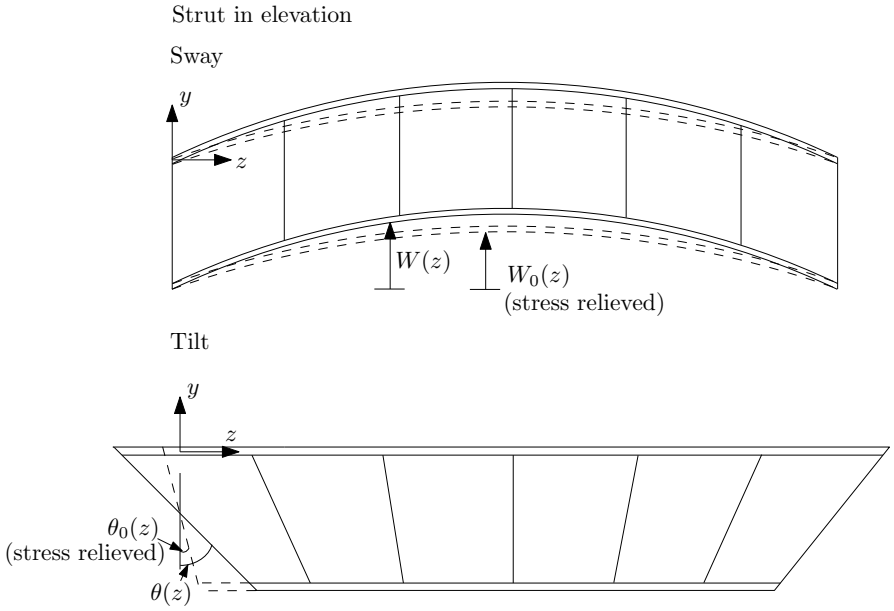


Figure 3: Global buckling modal components with (a) the sway component $W(z)$ and (b) the tilt component $\theta(z)$ shown about the global strong axis, along with their respective geometric imperfections $W_0(z)$ and $\theta_0(z)$.

expressions are written thus:

$$W(z) = q_s L \sin\left(\frac{\pi z}{L}\right), \quad \theta(z) = q_t \pi \cos\left(\frac{\pi z}{L}\right),$$
$$W_0(z) = q_{s0} L \sin\left(\frac{\pi z}{L}\right), \quad \theta_0(z) = q_{t0} \pi \cos\left(\frac{\pi z}{L}\right). \tag{1}$$

Out-of-plane and in-plane deflected shapes are also defined for the local modes. The in-plane deflected shape is assumed to be constant in the x-axis and varies linearly with the y-axis, in keeping with Timoshenko beam theory; this is used in the current formulation since shear strains have been shown to be essential for capturing interactive buckling behaviour [15]. The local out-of-plane deflection shapes are selected such that they give a good representation of the deflected shape of the element in the transverse direction, while also satisfying the boundary conditions given by the joints in the cross-section. The local buckling modes can be expressed mathematically thus:

$$u_{fl}(x,z) = u_f(z), \quad u_{wl}(y,z) = -\left(\frac{y}{h}\right) u_w(z),$$

$$w_{fl}(x,z) = f(x)w_f(z) = -\left(\frac{2x}{b}\right),$$
$$w_{wl}(y,z) = g(y)w_w(z) = \left[\frac{\pi}{2} + \frac{\pi y}{h} - \sin\left(\frac{\pi y}{h}\right) - \frac{\pi}{2}\cos\left(\frac{\pi y}{h}\right)\right] w_w(z), \tag{2}$$

where u is an in-plane deflection in the z-direction and w is an out-of-plane deflection. The subscript 'fl' indicates a local flange deflection and subscript 'wl' indicates a local web deflection. Both global and local buckling modes are shown in Fig. 4.

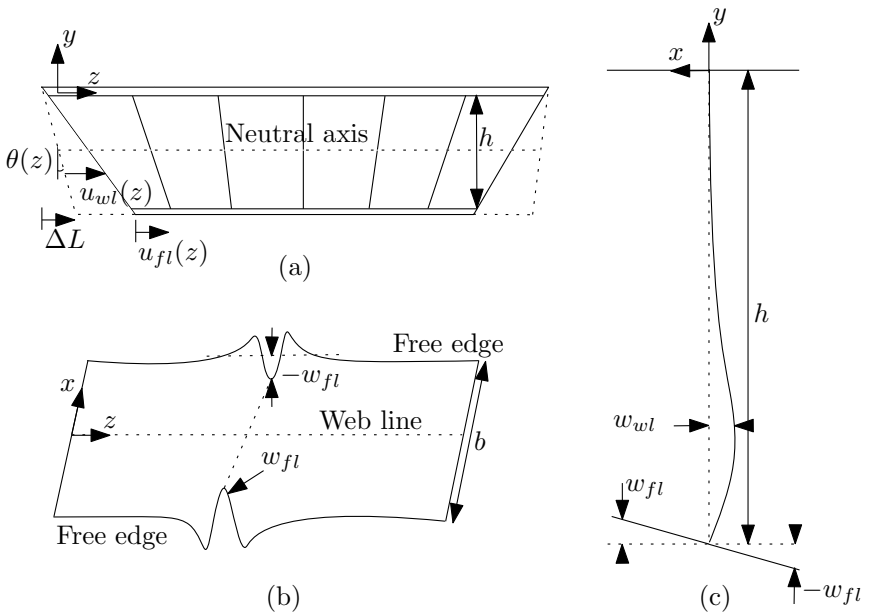


Figure 4: Local buckling modes for the I-section strut showing (a) the in-plane buckling mode, (b) the out-of-plane buckling mode in the flange and (c) the out-of-plane buckling mode in the flange and the web.

2.2. Total potential energy

The total potential energy V is a summation of several energy components of the strut, each formulated separately and presented currently. The complete derivation can be found in the authors' previous work [14] and is not presented currently for brevity. Note also that as the strut buckles in the global mode first, one flange will always be in more compression than the other, shown in the 'tilt' diagram in Figs. 3 and 4(c). It is therefore assumed that no local displacements occur in the less compressed flange during post-buckling.

First, the strain energy stored in bending U_B due to global buckling about the strong axis is given by the expression:

$$U_B = 2\int_0^L \frac{EI_f}{2}\left(\frac{\mathrm{d}^2W}{\mathrm{d}z^2} - \frac{\mathrm{d}^2W_0}{\mathrm{d}z^2}\right)^2 \mathrm{d}z, \tag{3}$$

where $I_f = bt_f^3/12$ being the second moment of area of the flange about its local neutral x-axis. Note that the global bending energy has been multiplied by two to account for both top and bottom flanges. The local bending energy contributions from the flange U_{bf} and from the web U_{bw} are determined by the respective expressions:

$$U_{bf} = \frac{D_f}{2}\int_0^L \int_{-b/2}^{b/2} \left\{ \left(\frac{\partial^2 w_{fl}}{\partial x^2} + \frac{\partial^2 w_{fl}}{\partial z^2}\right)^2 - 2(1-\nu)\left[\frac{\partial^2 w_{fl}}{\partial x^2}\frac{\partial^2 w_{fl}}{\partial z^2} - \left(\frac{\partial^2 w_{fl}}{\partial x \partial z}\right)^2\right] \right\} \mathrm{d}x\,\mathrm{d}z,$$
$$U_{bw} = \frac{D_w}{2}\int_0^L \int_{-h}^{0} \left\{ \left(\frac{\partial^2 w_{wl}}{\partial y^2} + \frac{\partial^2 w_{wl}}{\partial z^2}\right)^2 - 2(1-\nu)\left[\frac{\partial^2 w_{wl}}{\partial y^2}\frac{\partial^2 w_{wl}}{\partial z^2} - \left(\frac{\partial^2 w_{wl}}{\partial y \partial z}\right)^2\right] \right\} \mathrm{d}y\,\mathrm{d}z. \tag{4}$$

The parameters $D_f = Et_f^3/[12(1-\nu^2)]$ and $D_w = Et_w^3/[12(1-\nu^2)]$ represent the flexural rigidities of the flange and web respectively. The membrane energy from direct strain in the flanges can be found from the expression:

$$U_{\epsilon f} = \frac{1}{2}Et_f \int_0^L \int_{-b/2}^{b/2} \left(\epsilon_{z1}^2 + \epsilon_{z2}^2\right) \mathrm{d}x\,\mathrm{d}z, \tag{5}$$

where the direct strain components in the more and less compressed flanges (associated with subscripts 1 and 2 respectively) are given by the expressions:

$$\epsilon_{z1} = \frac{h}{2}\left(\dot{\theta} - \dot{\theta}_0\right) - \Delta + \frac{\partial u_{fl}}{\partial z} + \frac{1}{2}\left(\frac{\partial w_{fl}}{\partial z}\right)^2,$$
$$\epsilon_{z2} = -\frac{h}{2}\left(\dot{\theta} - \dot{\theta}_0\right) - \Delta, \tag{6}$$

where dots denote differentiation with respect to z and Δ is the uniform in-plane compressive strain. Note that the more compressed flange has no local buckling terms since it is assumed to experience no local deflections throughout the post-buckling range. The local buckling terms present in the strain expression for the more compressed flange are derived from von Kármán plate theory [16]. Similarly, the direct strain energy contribution to the total potential energy from the web is defined by the expression:

$$U_{\epsilon w} = \frac{1}{2}Et_w \int_0^L \int_{-h}^{0} \epsilon_{zw}^2 \,\mathrm{d}y\,\mathrm{d}z, \tag{7}$$

where the total direct strain in the web is given by:

$$\epsilon_{zw} = \frac{\partial u_t}{\partial z} - \Delta + \frac{\partial u_{wl}}{\partial z} + \frac{1}{2}\left(\frac{\partial w_{wl}}{\partial z}\right)^2. \tag{8}$$

Here, $u_t = (y + h/2)(\theta - \theta_0)$, which gives a linear distribution of the tilt component for the global buckling mode with a magnitude of zero at the neutral axis. The shear strain energy contribution from the more compressed flange is defined:

$$U_{\gamma f} = \frac{1}{2}Gt_f \int_0^L \int_{-b/2}^{b/2} \gamma_{xz}^2 \,\mathrm{d}x\,\mathrm{d}z, \tag{9}$$

where the flange shear strain term γ_{xz} is:

$$\gamma_{xz} = \frac{\partial u_{fl}}{\partial x} + \frac{\partial w_{fl}}{\partial z}\frac{\partial w_{fl}}{\partial x}. \tag{10}$$

This expression can be simplified by noting that the flange in-plane displacement u_{fl} is uniform in x and hence the first term is zero. Note that there is no shear strain energy arising from the less compressed flange since it is assumed to undergo no local deflections during post-buckling. The potential energy contribution due to shear strain in the web is given by the expression:

$$U_{\gamma w} = \frac{1}{2}Gt_w \int_0^L \int_{-h}^0 \gamma_{yz}^2 \,\mathrm{d}y\,\mathrm{d}z, \tag{11}$$

where the shear strain in the web γ_{yz} is defined thus:

$$\gamma_{yz} = \frac{\partial\left(W - W_0\right)}{\partial z} - \left(\theta - \theta_0\right) + \frac{\partial u_{wl}}{\partial y} + \frac{\partial w_{wl}}{\partial y}\frac{\partial w_{wl}}{\partial z}. \tag{12}$$

Note that in Equation (10), the first two terms that appear in Equation (12) are omitted from the shear strain expression for the flange since there are no global deflections in the x-direction. Moreover, there are no significant shear strains in the yz-plane (γ_{yz}) in the flange because it is thin.

The work done by the load term contributing to the total potential energy is expressed as the load P multiplied by the distance moved by the load in the same direction. It comprises terms global and local buckling with pure axial compression and is written thus:

$$P\mathcal{E} = P\int_0^L \left[\frac{q_s^2\pi^2}{2}\cos^2\left(\frac{\pi z}{L}\right) - \frac{1}{2}\dot{u}_w + \Delta\right]\mathrm{d}z. \tag{13}$$

The individual components presented in Equations (3)–(13) can be accumulated to give the total potential energy in its most general form thus:

$$V = U_B + U_{bf} + U_{bw} + U_{\epsilon f} + U_{\epsilon w} + U_{\gamma f} + U_{\gamma w} - P\mathcal{E}. \tag{14}$$

2.3. Modelling simplification

A relationship between the out-of-plane displacements in the longitudinal direction of the flange w_f and the web w_w can be established to simplify the model significantly. By considering the two deflections, a scaling parameter κ is defined such that $w_w(z) = \kappa w_f(z)$. The parameter κ is determined by the rigidity of the joint connecting the flange and the web. This gives the result $\kappa = -h/(\pi b) \equiv \kappa_0$ if the joint is assumed to provide full rotational continuity and is found by equating the rotation of the flange and the web at the location of the joint, using the first derivative of the displacement shapes defined previously in Equation (2).

In reality, this is an upper bound on the joint stiffness since the functions f and g are approximations. Hence, κ is a correction factor to account for the various simplifications made in terms of assumed functional forms and that the less compressed flange does not

deflect. Moreover, it has the advantage that it does not affect the global buckling response. The local buckling load given by the analytical model was calibrated in [14] using the buckling load given by the FE model, described later in the current work. It was established that $\kappa = 0.65\kappa_0 \equiv \kappa_c$ gave the most numerically accurate description of the rigidity of the flange–web joint. Once κ is evaluated, the two out-of-plane displacements can be replaced by a single function w, where $w = w_f = w_w/\kappa$. Additionally, the in-plane displacements can be simplified by the relationship $u = u_f = u_w$, found by simply imposing continuity of the in-plane displacement at the flange–web joints. The number of functions that need to be solved are therefore reduced significantly, simplifying the equations and increasing computational efficiency.

2.4. Governing equations

The governing equations of equilibrium can be obtained from minimizing the total potential energy V by performing the well known procedure of the calculus of variations [17]; V is expressed in the Lagrangian form thus:

$$V = \int_0^L \mathcal{L}\left(\ddot{w}, \dot{w}, w, \dot{u}, u, z\right) \mathrm{d}z, \tag{15}$$

with the first variation being written as:

$$\delta V = \int_0^L \left\{ \frac{\partial \mathcal{L}}{\partial \ddot{w}}\delta\ddot{w} + \frac{\partial \mathcal{L}}{\partial \dot{w}}\delta\dot{w} + \frac{\partial \mathcal{L}}{\partial w}\delta w + \frac{\partial \mathcal{L}}{\partial \dot{u}}\delta\dot{u} + \frac{\partial \mathcal{L}}{\partial u}\delta u \right\} \mathrm{d}z. \tag{16}$$

Equilibrium is defined when V is stationary, hence the first variation must vanish for all small changes of w and u, resulting in the Euler–Lagrange equations. These comprise a fourth order nonlinear ordinary differential equation (ODE) in w and a second order nonlinear ODE in u:

$$\begin{aligned} &\frac{\mathrm{d}^2}{\mathrm{d}z^2}\left(\frac{\partial \mathcal{L}}{\partial \ddot{w}}\right) - \frac{\mathrm{d}}{\mathrm{d}z}\left(\frac{\partial \mathcal{L}}{\partial \dot{w}}\right) + \frac{\partial \mathcal{L}}{\partial w} = 0, \\ &\frac{\mathrm{d}}{\mathrm{d}z}\left(\frac{\partial \mathcal{L}}{\partial \dot{u}}\right) - \frac{\partial \mathcal{L}}{\partial u} = 0. \end{aligned} \tag{17}$$

Corresponding integral equations can also be obtained by considering the first partial derivatives of V with respect to the generalized coordinates q_s and q_t, and additionally the generalized coordinate defining the purely compressive displacement Δ and setting each derivative to zero. The boundary conditions for a simply supported strut are then applied to the set of governing equations, assuming symmetric displacements about the midspan. They are written thus:

$$w(0) = \ddot{w}(0) = \dot{w}(L/2) = \dddot{w}(L/2) = u(L/2) = 0, \tag{18}$$

with an additional boundary condition imposed at the point of loading, to match the in-plane strain. Note that the global buckling load P_o^{C} can be determined by considering the

Hessian matrix of the total potential energy V at the fundamental (pre-buckling) state F (i.e. w and u with all their derivatives being zero) and so:

$$\mathbf{V}_{ij}^{\mathrm{F}} = \begin{bmatrix} \left.\frac{\partial^2 V}{\partial q_s^2}\right|^{\mathrm{F}} & \left.\frac{\partial^2 V}{\partial q_s \partial q_t}\right|^{\mathrm{F}} \\ \left.\frac{\partial^2 V}{\partial q_t \partial q_s}\right|^{\mathrm{F}} & \left.\frac{\partial^2 V}{\partial q_t^2}\right|^{\mathrm{F}} \end{bmatrix}. \tag{19}$$

The matrix is singular at the global critical load P_o^{C}. This leads to the expression:

$$P_o^{\mathrm{C}} = \frac{2EI_f\pi^2}{L^2} + \frac{G(t_w h + 6t_f b)}{1 + 6t_f b/(t_w h) + 12GL^2/(E\pi^2 h^2)}. \tag{20}$$

Full details about the formulation may be found in [14] where the full nonlinear differential and integral equations of equilibrium are presented explicitly.

3. Finite element model

Varying the strut length and the cross-section height is anticipated to have an effect on the relative global and local buckling loads of the strut, implying that for some lengths or cross-section heights, local buckling could become critical. An analytical model has been previously presented which can account for the case where local buckling is critical [14]. However, the equations become more complex and difficult to solve numerically for the post-buckling range. Given that FE models constructed in the commercial software package ABAQUS [18] have previously provided a successful comparison to similar analytical models, particularly for the ultimate loads when either global or local buckling is critical [19, 13], it is known to be acceptably accurate and, in this case, much more convenient to use FE in the parametric study, for cases where local buckling is critical.

A four-noded shell element with reduced integration is selected from the ABAQUS library (S4R) which allows the elements to bend in double curvature and has been shown previously to be applicable to problems with geometric nonlinearities [20]. The strut is meshed with a uniform element size of 10 mm in the longitudinal direction, by 5 mm in the transverse direction and has been previously demonstrated to provide a sufficient degree of accuracy for acceptable computational costs [13]. The strut is created in three individual parts: the two flanges and the web with the centreline of the top and bottom flanges being tied rigidly to the top and bottom edges of the web. Only one half of the strut is modelled with symmetry imposed at mid-span to reduce computational costs; this also matches the symmetry condition imposed by the analytical model. A simply supported boundary condition is also imposed at the end of the strut and the load is applied as a concentrated force at the centroid of the cross-section. Initially, linear eigenvalue analysis is used to determine the buckling modes of the strut and their respective load capacities. The first global and local modes are then input into a nonlinear Riks analysis [21] as nominal initial geometric imperfections that are sufficiently small to mimic the perfect behaviour. This allows for post-buckling behaviours to be simulated using static methods in ABAQUS.

4. Solution strategy

4.1. Varying the strut length

The parametric study uses the ODEs and accompanying set of integral equations presented in §2.4 for the cases where global buckling is critical. First, the perfect case strut is investigated, hence all terms associated with an initial imperfection (*i.e.* all terms with subscript '0') are set to zero. The length is then varied parametrically in order to determine the post-buckling behaviour of the strut for each geometry, and any boundaries where the behaviour changes characteristics distinctly. The change in global slenderness is anticipated to affect the global buckling load but have an insignificant influence on the local buckling load of the strut. When the length is such that global and local buckling loads are relatively close, it is expected that interactive behaviour will be observed and the length where global and local buckling loads become coincident is defined as L_c. When the lengths are such that the global and local buckling loads are very different, it is expected that other issues such as plastic deformations or serviceability concerns would begin to become apparent before any interaction is observed. In this way, the lengths L_o and L_l can be determined, denoting the boundaries where global buckling or local buckling only are observed in the elastic range respectively.

The study of struts with a length that induces critical global buckling is conducted analytically using the software AUTO-07P and lengths are varied using the numerical continuation functionality. The study for struts that have a length inducing critical local buckling is conducted in the FE software ABAQUS, using the model described in §3. In order to simulate buckling in the FE model using static methods, an initial geometric imperfection must be introduced into the nonlinear Riks analysis, thus to make fair comparisons between the FE and analytical methods, these geometric imperfections must be kept to be as small as possible and can be regarded as a small perturbation purely to induce the near-perfect post-buckling behaviour. It is found that a nominal global imperfection of $L/80000$ and a nominal local imperfection of $t_f/600$ are sufficient to ensure buckling is observed in the strut for most lengths. However, it was necessary to increase these imperfection sizes by a very small amount to simulate buckling in much shorter struts.

The effect of a significant initial global geometric imperfection on the strut is also considered and incorporated into the parametric study. The initial normalized out-of-straightness amplitude q_{s0} (and by implication q_{t0}) is increased parametrically in AUTO-07P to the values 1/1500 and 1/500, representing measured and design manufacturing tolerances given by previous studies and design guidelines [22, 23]. This can be simulated in the FE model by increasing the nominal global imperfection to more realistic values of $L/1500$ and $L/500$, respectively. The parametric study is then repeated for struts with the more realistic imperfections to observe their effects.

4.2. Varying the cross-section height

A similar methodology is used to conduct the parametric study on varying cross-section heights, as that described in §4.1. However, varying the cross-section height differs in that it modifies both the global and local buckling loads of the strut. Crucially, this modification

changes the previously defined relationship between the out-of-plane displacement of the flange and the web, namely the parameter κ. Therefore, it is necessary for κ to be re-calibrated using the FE model, for each cross-section height investigated. When conducting the parametric study, the appropriate κ value is therefore used for each corresponding cross-section height h, found from the calibration process. The cross-section height is then varied to investigate the post-buckling behaviour of the strut for each geometry and transition points between regions of distinct post-buckling behaviours are identified. The cross-section height where global and local buckling loads are coincident is termed h_c and it is expected that the interactive region would occur between $h_o < h < h_l$, using similar notation as defined in §4.1 for varying the strut length (*i.e.* lengths L_o and L_l respectively).

4.3. Deflection and strain criteria

The lengths L_o and L_l and cross-section heights h_o and h_l are defined as when unacceptably high deflections develop in the strut before any mode interaction is observed in the elastic range. Hitherto, the strut has been assumed to remain elastic and a solely deflection based criterion was used to define the point that rendered the strut in violation with serviceability requirements [12]. To define L_o and h_o, when global buckling is critical, the current study is based on a fairly arbitrary value of $q_s = q_s^{\mathrm{D}}$ as a large global lateral deflection; *i.e.* when $q_s > q_s^{\mathrm{D}}$, which is defined currently as $q_s^{\mathrm{D}} = 1/100$, and the local buckling mode is yet to be activated, the strut can be considered to be buckling in a purely global mode. Similarly, when local buckling is critical and the path is weakly stable, the ultimate load is considered to be reached when the out-of-plane deflection of the cross-section at midspan exceeds $3t_f$, while in the elastic range.

However, for defining the length L_l and cross-section height h_l, it is highly important for practical design to know when plasticity is first observed in the component. This is especially important when local buckling is critical since it is well known that failure mechanisms are governed by plasticity in stocky columns and by elastic buckling in more slender columns. Plasticity is much more likely to affect the load carrying capacity of the strut for cases where local buckling is critical since the strains within the locally buckled flange or web plates are much more likely to exceed the material yield stress at some stage. It is therefore useful to define an additional strain based criterion to identify the ultimate loads where first yield is first observed, for the case where local buckling is critical. A high yield stress of $\sigma_{\mathrm{y}} = 960\,\mathrm{N/mm^2}$ is considered currently, partially to keep elasticity considerations as the primary focus but also to reflect the recently increasing popularity of using high strength steels in construction [24]. Plastic deformation of the strut is considered to occur when any element of the strut mesh in ABAQUS exceeds the yield stress, and this criterion can also be used to estimate the ultimate load of the strut. A sketch of the expected trends to be observed from the parametric variations is shown in Fig. 5.

5. Numerical studies

The effect of varying the strut length L and the cross-section height h are examined in turn through two independent parametric studies using methods discussed in §4. The

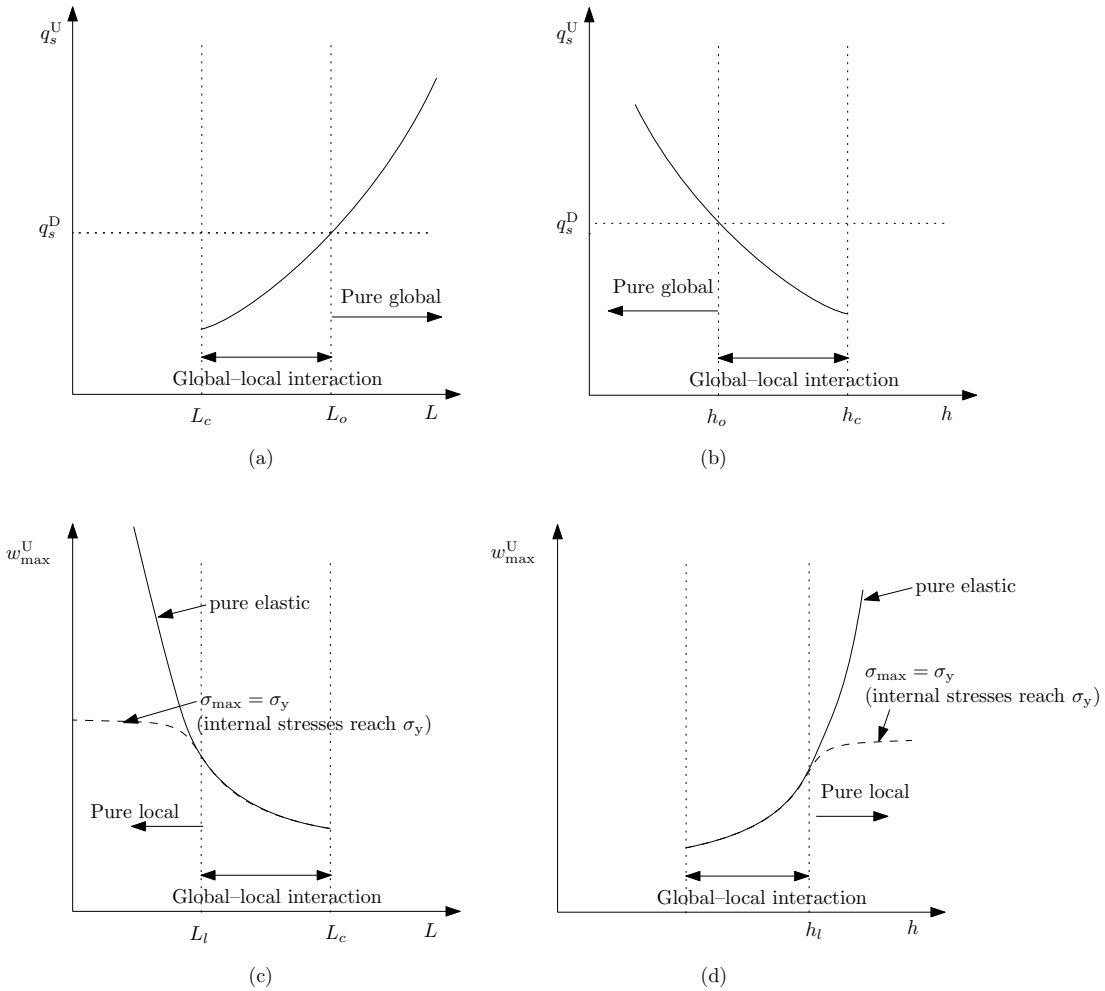


Figure 5: Sketch of the parametric variations and the expected post-buckling response. Variations of (a) length and (b) cross-section height when global buckling is critical. Variations of (c) length and (d) cross-section height when local buckling is critical.

material and cross-sectional geometric properties of the strut selected for the studies are detailed in Table 1. For varying the strut lengths, the cross-section height is kept con-

Young's Modulus E	$210000\,\mathrm{N/mm^2}$
Poisson's Ratio ν	0.3
Flange breadth b	90 mm
Flange thickness t_f	2.4 mm
Web thickness t_w	2.4 mm

Table 1: Geometric and material properties of the strut, for the parametric studies of varying strut lengths and cross-section heights.

stant at 100 mm and for varying cross-section heights, the strut length is kept constant at 4000 mm.

The process of varying the strut length L is relatively straightforward. However, in changing the cross-section height h, the relative mutual interaction between the flange and the web also changes because the expression in Eq. (2) for the web is approximation that is based on the shape of a strut with one end pinned and the other fixed. Therefore, the parameter κ linking, the out-of-plane deflections between the flange and the web, also needs to be re-calibrated, as mentioned previously for each h value, in order to give an accurate local buckling load prediction for each cross-section geometry. The calibrated values κ_c found are shown in Fig. 6; Fig. 6(a) shows that κ_c reduces for a smaller cross-section

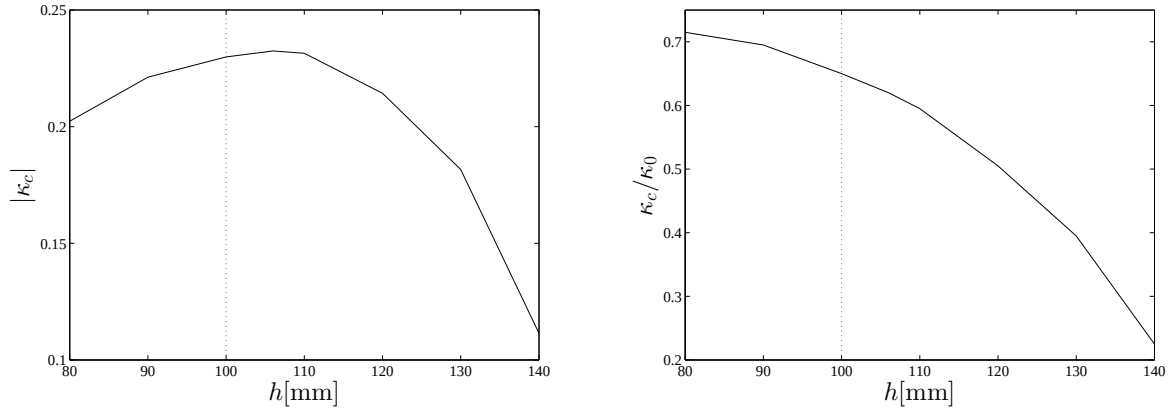


Figure 6: The effect of varying web heights on the calibrated parameter κ_c where $w_f = \kappa_c w_w$. Graphs show (a) the magnitude of κ_c and (b) κ_c relative to the fully rigidly rotating flange–web joint ($\kappa = \kappa_0$), versus the cross-section height. The dotted line indicates the cross-section height of $h = 100$ mm used in the parametric study of varying the strut length.

height. Here, the web is relatively stocky and as the flange deflects, the web is unable to deflect fully in sympathy. Therefore, as the cross-section height is decreased, the effect of the flange on the web is also decreased. When h lies between 100 mm to 110 mm, κ_c reaches a peak as the flange and the web begin to have similar critical buckling loads and have the greatest effect on each other. When $h > 110$ mm, κ_c decreases rapidly. The flange and web begin to act individually as plated components again and have a reduced mutual influence, this time the web having increasingly less influence on the flange. The geometry of the increasing cross-section height also dictates that an increasingly smaller out-of-plane deflection would be observed at the mid-point of the web for an unchanged flange geometry, assuming a rigidly rotating flange–web connection, resulting in a decreased κ_c parameter. Figure 6(b) gives an indication of the rigidity of the flange–web connection, relative to the fully rigidly rotating case of $\kappa_0 = -h/(\pi b)$. For a shallower cross-section with a stocky web, the flange–web joint is closer to being fully rigid and for a deeper web, the flange–web joint moves closer to becoming fully pinned. It is worth emphasizing that the κ_c parameters found currently are used in the parametric study of varying cross-section heights.

5.1. Results

The parametric study reveals that strong axis global–local mode interaction occurs between $L_l < L < L_o$ and $h_o < h < h_l$ for the varying of strut lengths and cross-section heights, respectively. For the geometries given in Table 1, it is found that $L_l = 2646$ mm, $L_o = 4950$ mm, $h_o = 84$ mm and $h_l = 145$ mm. The lengths and cross-section heights that fall outside of this region are classified as not undergoing an interactive post-buckling response, using the deflection and strain based criterion discussed in §4.3. The critical buckling length L_c is found by the analytical model to be $L_c = 3340$ mm, where $P_o^{\mathrm{C}} = P_l^{\mathrm{C}}$. The FE model determines L_c to be 3430 mm where the global and local buckling loads are approximately equal in a linear eigenvalue analysis, this represents a difference of only 2.6% between the analytical and FE solutions for the critical length, giving a very good comparison. Similarly, the critical cross-section height h_c is found to be 116 mm by both the analytical and FE models.

The results of the parametric studies for these given geometries are presented in Fig. 7(a) for the strut length and Fig. 7(b) for the cross-section height. It can be observed that when global buckling is critical, *i.e.* when $L > L_c$ or $h < h_c$, the load carrying capacity is equal to the global buckling load $P_u = P_o^{\mathrm{C}}$ as the global buckling mode is only weakly stable. When local buckling is critical, *i.e.* when $L < L_c$ or $h > h_c$, the load carrying capacity is able to reach higher loads than the local buckling load P_l^{C} since the local buckling mode has a strongly stable post-buckling behaviour in the elastic range. However, the load carrying capacity is not able to reach the global buckling load P_o^{C} due to the strong axis global–local interaction in the region $L_l < L < L_c$ and $h_c < h < h_l$. It is also limited by the deflection of the compression flange $w_{\max} = 3t_f$ for even shorter elastic struts of $L < L_l$ and deeper cross-section heights $h > h_l$ as indicated by the solid line.

The graphs also show the results for the case where a material yield stress $\sigma_{\mathrm{y}} = 960\,\mathrm{N/mm^2}$ is taken into consideration, which is shown with the dot-dashed line in Figs. 7(a)

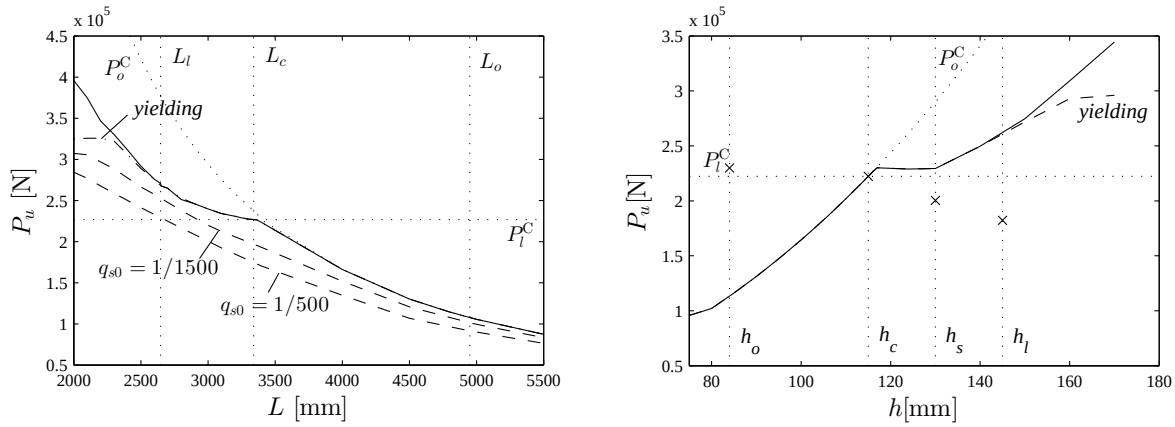


Figure 7: Graphs showing the ultimate load P_u versus (a) the strut length L and (b) the cross-section height h. The solid line represents the perfect elastic case, the dot-dashed line represents the perfect case including yielding and the dashed lines represent struts with a global out-of-straightness imperfection, with $q_{s0} = 1/1500$ and $q_{s0} = 1/500$, labelled accordingly. The vertical dotted lines indicate the transition lengths for the perfect case strut, separating regions of different post-buckling responses. Crosses in (b) represent the local buckling load for each transition height.

and (b). It can be observed that when the yielding limit is imposed, the load carrying capacity of the strut is decreased and reaches a plateau at $P_u = 325\,\mathrm{kN}$ for the variation of strut length. This is approximately $0.5P_\mathrm{y}$ where P_y is the failure load due to pure squash, assuming a yield stress of $\sigma_\mathrm{y} = 960\,\mathrm{N/mm^2}$. A similar plateau is reached at $P_u = 300\,\mathrm{kN}$ for the variation of cross-section height, which is also approximately $0.35P_\mathrm{y}$; however as the cross-section height increases, the material limit is reached for a lower proportion of P_y since the cross-sectional area A increases with the increasing cross-section height.

The effects of initial global imperfections on the load carrying capacity are also investigated. Figure 7(a) shows two dashed lines, indicating the post-buckling behaviour of a strut with an initial, stress relieved global out-of-straightness of $q_{s0} = 1/1500$ and $q_{s0} = 1/500$, labelled accordingly. A reduced load carrying capacity is found as the magnitude of the initial imperfection increases, and it can be seen from Fig. 7(a) that this effect is more pronounced in the region where global–local interaction is observed. This is similar to the findings in earlier work by van der Neut [5], where it was found that the 'imperfection sensitive' regions are those where the global and local buckling loads are close. Similar trends are exhibited by both parametric studies and it is observed that the characteristics of the post-buckling response are dominated by the relative global and local buckling loads, as well as the material yield limit. Therefore, it can be deduced that the sensitivity of the strut to global imperfections for the variation of cross-section heights would exhibit similar behaviour to that found for the variation of lengths, and therefore has not been analysed

in detail presently. It is expected that the strut would be most sensitive to initial global imperfections in the interactive region, and particularly at the critical cross-section height h_c.

The central graph in Fig. 8 is a transformation of the graph presented in Fig. 7(a) into a form similar to that presented by van der Neut [5], where the load carrying capacity P_u is plotted versus the global buckling load P_o^{C} for struts varying in length; both axes are normalized with respect to the local buckling load P_l^{C}, which remains constant throughout since it is basically invariant with length (at least for the lengths considered presently). The surrounding graphs show the equilibrium paths of the strut in different regions of the central graph, with the important strut lengths labelled. A similar transformation of Fig. 7(b) is presented in Fig. 9 for the varying of cross-section heights. Additionally, note that, unlike the parametric study of strut lengths, the graph in Fig. 9 has been normalized with respect to a changing P_l^{C} value, as the local buckling load changes with the cross-section height.

It can be seen that at $L = L_c = 3340\,\mathrm{mm}$ and $h = h_c = 116\,\mathrm{mm}$ the global and local buckling loads are equal with the critical and secondary bifurcation points being triggered simultaneously. This results in an extremely unstable, potentially explosive, post-buckling response and reflects previous work conducted in the field of interactive buckling, where it has been said that the 'most optimum' design, *i.e.* when the buckling loads are all very similar, can in fact have severe consequences. The configuration for which this occurs has been famously termed as the 'naive optimum' [2].

For the ranges $L_c < L < L_o$, and $h_o < h < h_c$, the equilibrium paths show a neutrally stable post-buckling path where global buckling is triggered, followed by an unstable post-buckling path at a secondary bifurcation point, where local buckling is also triggered and interacts with the global mode. For the parametric ranges $L_l < L < L_c$ and $h_c < h < h_l$, the equilibrium path shows an initially stable post-buckling path where local buckling is triggered first. At the secondary bifurcation point, global buckling is also triggered and the equilibrium path becomes interactive and unstable. Outside of the interactive region, it can be seen that when $L > L_o$ and $h < h_o$, the equilibrium path exhibits a neutrally stable path, where only global buckling is active. Similarly, when $L < L_l$ and $h > h_l$, the equilibrium path is stable and only local buckling is active. The effects of the global out-of-straightness imperfections on the equilibrium paths can be further observed in Fig. 8 for the variation of strut lengths, and it is fair to assume they would have a similar effect while varying the cross-section height. It can be seen clearly that the presence of the imperfection decreases the load carrying capacity of the strut. Note that the global imperfection appears to have a much larger effect on the post-buckling path for the cases where global buckling is critical.

An additional region, defined by h_s is identified in the variation of cross-section heights. Figure 9 shows that for $h_c < h < h_s$, the post-buckling path is initially stable and while buckling in the local mode, becoming strongly unstable when the interaction with the global buckling mode is triggered at the secondary bifurcation point. However, for the range $h_s < h < h_l$, interaction with the global buckling load is also observed but the post-buckling behaviour following the secondary bifurcation point is approximately neutral.

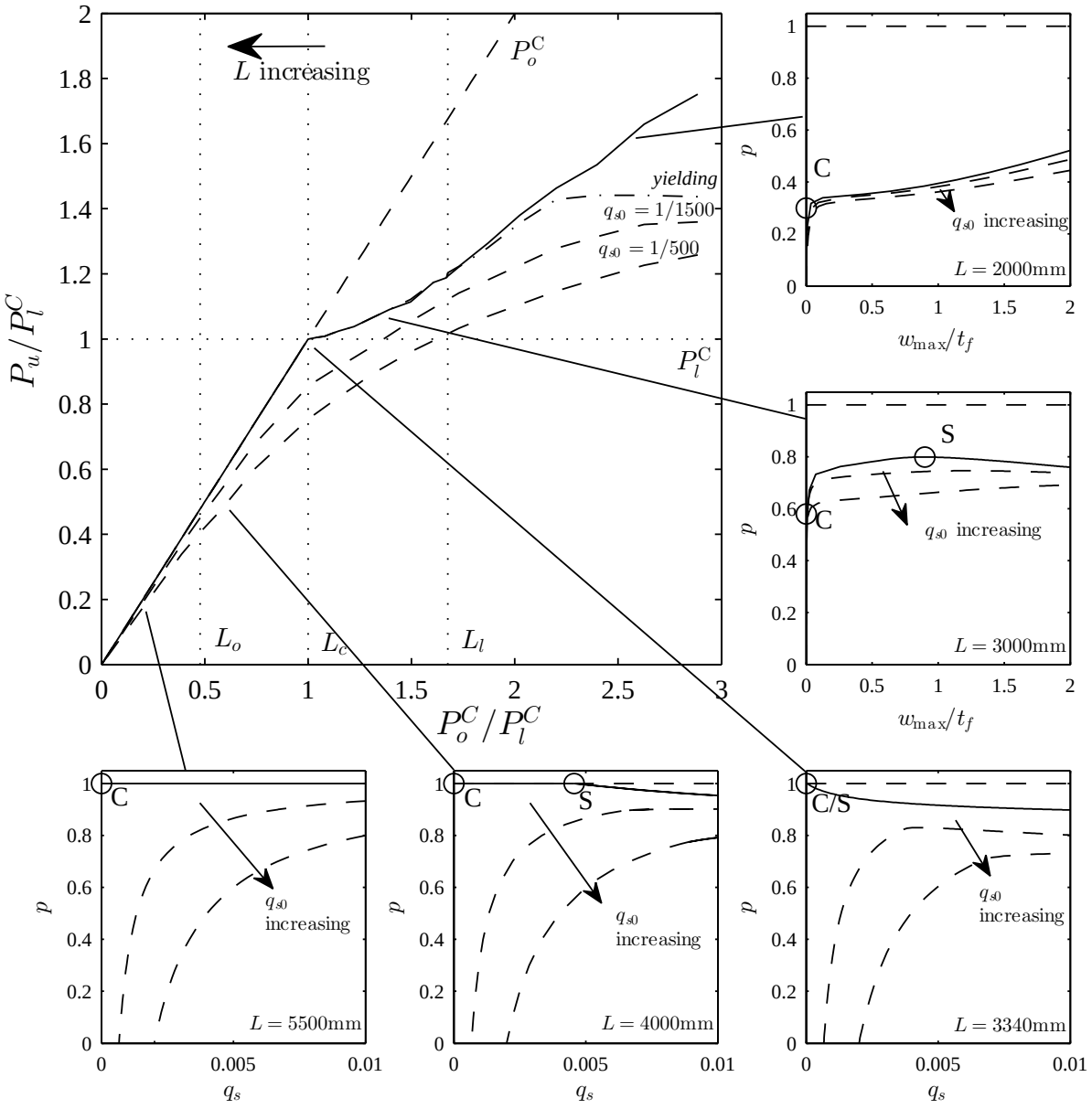


Figure 8: The principal graph shows the normalized ultimate load P_u/P_l^{C} of the strut versus the normalized global buckling load $P_o^{\mathrm{C}}/P_l^{\mathrm{C}}$ while varying strut lengths L. The solid line represents the perfect elastic case, the dot-dashed line represents the case including material yield and the dashed lines are for cases where initial global imperfections exist, labelled accordingly with $q_{s0} = 1/1500$ and $q_{s0} = 1/500$. The surrounding graphs correspond to equilibrium paths plotted for different regions of the central graph, separated by the vertical dotted lines; critical and secondary bifurcation points are labelled 'C' and 'S' respectively with the normalized load $p = P/P_o^{\mathrm{C}}$.

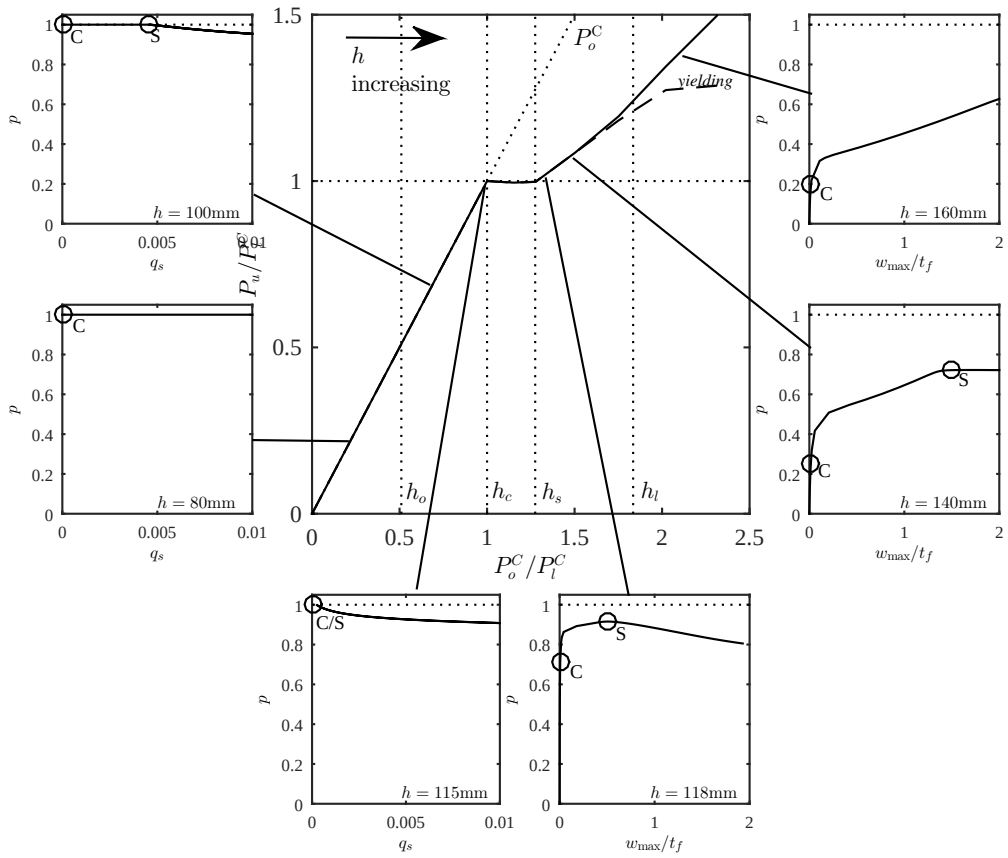


Figure 9: The principal graph shows the normalized ultimate load P_u/P_l^{C} versus the normalized global buckling load $P_o^{\mathrm{C}}/P_l^{\mathrm{C}}$ while varying the cross-section height h. The surrounding graphs and lines are as defined in Fig. 8.

This corresponds with van der Neut's findings [5], where a region of neutral post-buckling behaviour is found for certain geometries in both cases where global or local buckling is critical. Note that there is no technical reason why a similar region could not be identified in the variation of the strut length. However, the exact location is difficult to identify, possibly owing to an intrinsically less distinct transition point or due to the application of initial imperfections in the FE model that were perhaps too large for the effect to be observed.

The central graphs in Figures 8 and 9 can be compared directly to Fig. 1 by approximating a line to replicate the dotted line in Fig. 1 joining the origin to the stable-neutral boundary. In this way, the $1/\Psi$ values of the current parametric studies may be determined, at least approximately. It is found that $1/\Psi \approx 1.6$, when varying both the length and height of the strut, thus $\Psi \approx 0.63$ for both cases, giving an expression of $(1 + \Psi)/(2\Psi) \approx 1.25$ to determine the boundary between the unstable to stable post-buckling behaviours. This corresponds well qualitatively to van der Neut's findings [5] and quantitatively to recent work conducted on I-section struts buckling globally about the weak axis [12]. It should be noted that the stiffness reduction factor Ψ is significantly higher than van der Neut's value of 0.41. However, it should be considered that, unlike van der Neut's idealized strut, the current model has included the deflection of the web within the cross-section. Hence, the interaction of the web with the flange would cause the strut to have a higher stiffness reduction factor when compared to a system where the plates are effectively simply-supported at their boundaries, as assumed in [5]. Moreover, the current model has been previously validated using an FE model developed in the software ABAQUS [14].

Figures 10(a) and (b) show the normalized global mid-span deflection at the ultimate load q_s^{U} versus the strut length and cross-section height for each parametric study, respectively. Note that the superscript U refers explicitly to the stated quantity at the ultimate load. In both figures, global buckling occurs first in the strut. It is observed that the mid-span displacement at the ultimate load reduces as the strut length approaches L_c and the cross-section height approaches h_c. When global buckling is critical, a decrease in the strut length has a negligible effect on the local buckling load, but increases the global buckling load. When varying the cross-section height, an increase in h increases the global buckling load while simultaneously decreasing the local buckling load. In both cases, the two separate buckling loads move closer together. Therefore, the lateral mid-span deflection is less developed before the the ultimate load is reached and local buckling destabilizes the system earlier in the post-buckling range. When $P_o^{\mathrm{C}} \approx P_l^{\mathrm{C}}$, the lateral deflection at mid-span is approximately zero at the ultimate load for both parametric studies, as would be expected.

Figures 10(c) and (d) show the maximum out-of-plane displacement in the flange at the ultimate load (for the interactive cases) and at the material stress limit (for the cases where local buckling only is found) for the variation of strut lengths and cross-section heights, respectively. All struts shown buckle in the local mode first. Since the local buckling load is basically invariant with strut length for the lengths considered in this study, this remains constant, but the global buckling load increases as the strut length decreases and the two loads diverge. When increasing the cross-section height, the global buckling load

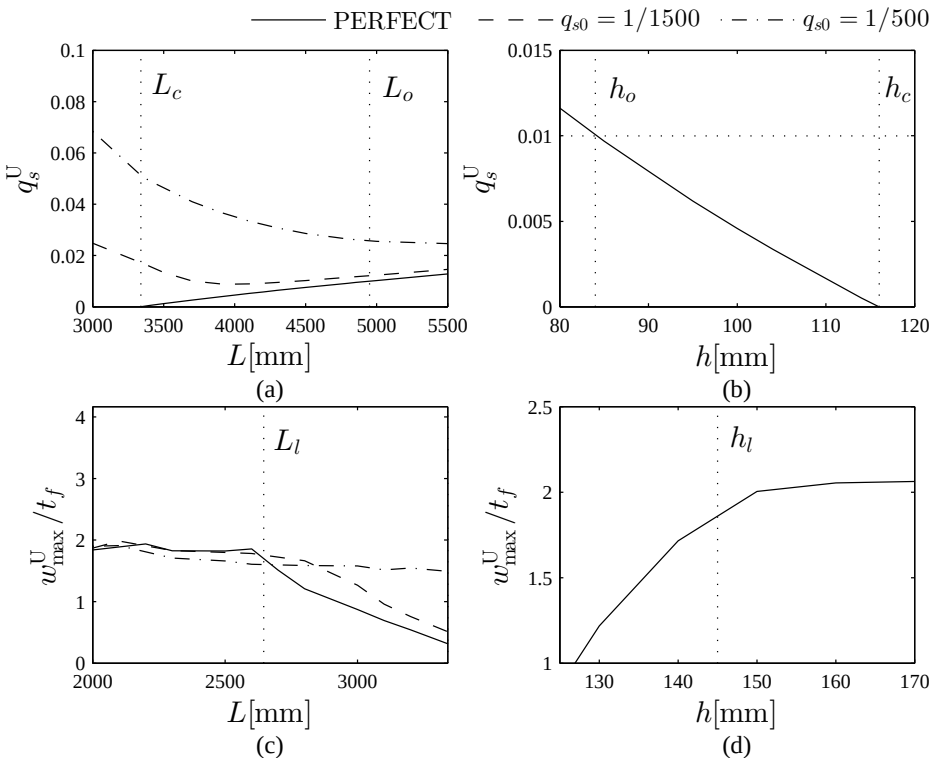


Figure 10: Results from the parametric study for the strut length L and cross-section height h varying. Graphs (a) and (b) show q_s^{U}, the normalized lateral displacement at the ultimate load, versus the respective varying geometric parameter. Graphs (c) and (d) show $w_{\max}^{\mathrm{U}}/t_f$, the local out-of-plane displacement at the ultimate load normalized with respect to the web thickness, plotted against the respective varying geometric parameter.

also increases while simultaneously decreasing the local buckling load. Therefore, in both cases, the local mode, and consequently the out-of-plane displacement, undergoes more development before the global buckling mode is activated and the ultimate load carrying capacity is reached. When $L < L_l$ and $h > h_l$, the out-of-plane displacement ceases to develop and reaches a plateau at approximately $w^{\mathrm{U}}_{\mathrm{max}} = 4.5\,\mathrm{mm}$ and $4.8\,\mathrm{mm}$ for the variation of strut length and cross-section heights respectively, indicating that the stress limit of the strut material has been reached.

The effect of the global geometric imperfection can also be observed from the parametric study where strut lengths are varied. Note that, as stated earlier, the similar trends found in both parametric studies indicate that the global geometric imperfections will have a very similar effect on the variation of cross-section heights. It can be seen from Fig. 10(a) that q_s^{U} increases with the presence of an initial global imperfection. The mid-span deflection q_s has a non-zero value pre-buckling, hence the equilibrium path is translated along the q_s-axis, shifting the peak load simultaneously, as can be seen in Fig. 11.

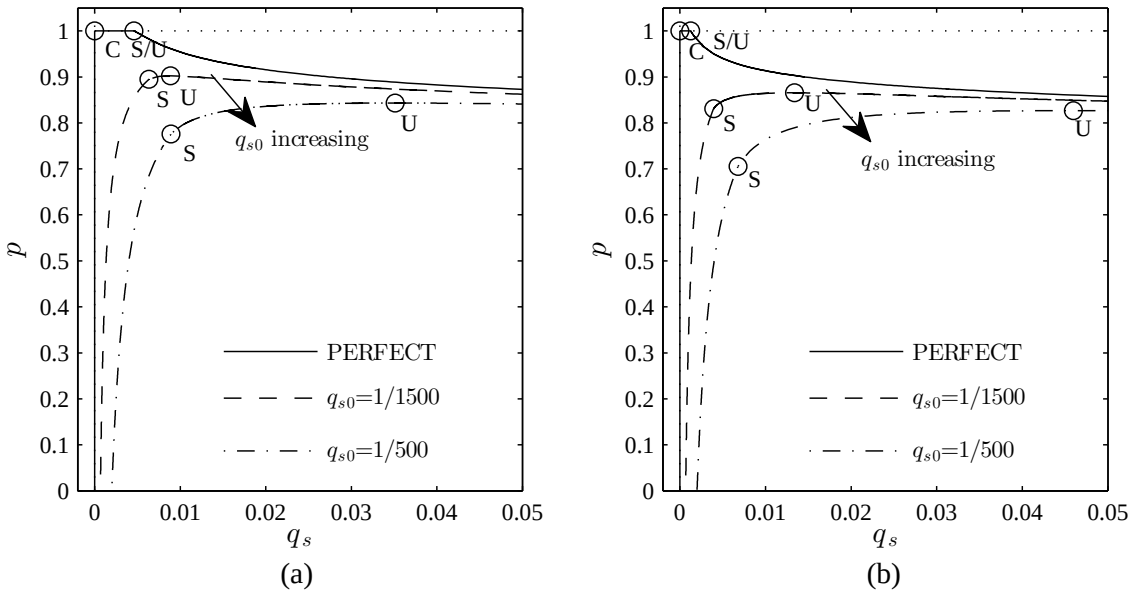


Figure 11: Equilibrium paths showing the normalized load $p = P/P_o^{\mathrm{C}}$ versus the non-dimensional mid-span deflection q_s for two example struts with lengths (a) 4000 mm and (b) 3500 mm. Critical bifurcations are marked C, secondary bifurcations are marked S and ultimate loads are marked U. Perfect and imperfect strut examples are shown and labelled accordingly.

Additionally, it was observed previously [14] that with a sufficiently large initial imperfection, all equilibrium paths converge to a neutrally stable state. Therefore, as this phenomenon develops, the ultimate load occurs further along the post-buckling path for increasing initial imperfections, until the imperfection becomes of sufficient magnitude such that a distinct peak load can no longer be observed. This effect is more pronounced for

shorter strut lengths and can be further observed in Fig. 11, which presents the equilibrium paths for two different strut lengths with increasing initial global geometric imperfections. The large increase in q_s^{U} for imperfect shorter lengths seen in Fig. 10(a) can also be attributed to this phenomenon.

For the case where local buckling occurs first, struts with longer lengths reach the elastic limit much quicker after the local mode develops for larger initial geometric imperfections, as evidenced in Fig. 10(c). Note that for the lengths 2000 mm to 2600 mm where the elastic limit is reached and the maximum midspan deflections begin to converge, the solutions for different imperfections appear to cross over. This is attributed to the meshing of the strut as well as the discretization of the solution in ABAQUS. However, on comparing with the relative magnitudes of the $w_{\mathrm{max}}^{\mathrm{U}}$ values at strut lengths outside of this range, it can be said for the range of lengths between 2000 mm to 2600 mm, that $w_{\mathrm{max}}^{\mathrm{U}}$ is effectively converging to the same value and that any discrepancies due to the FE modelling assumptions are not significant.

The effect of the global geometric imperfection can be further observed by considering the global lateral displacement at the secondary bifurcation point, for the case where global buckling is critical. Figure 12 shows the global midspan displacement of the strut at the

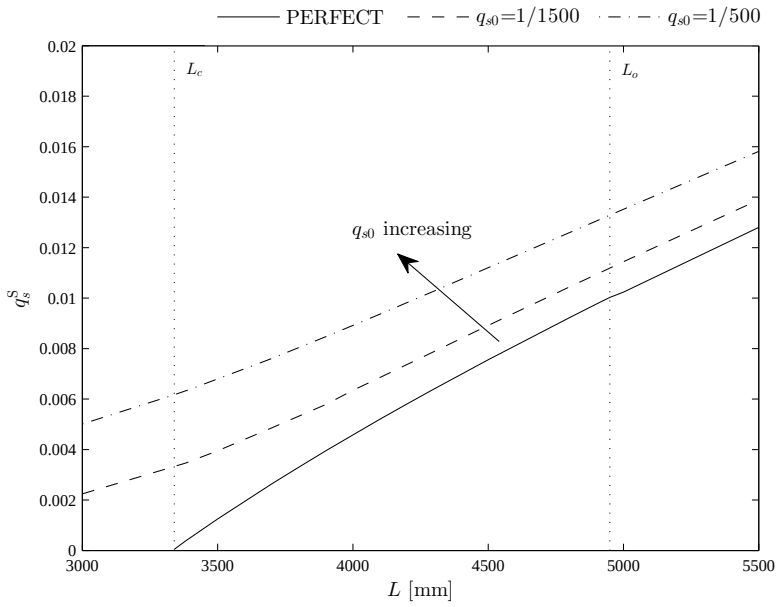


Figure 12: Normalized lateral midspan displacement of the strut at the secondary bifurcation point q_s^{S} for both perfect struts (solid line) and struts with initial global geometric imperfections versus the strut length L. All lengths of strut shown buckle globally first.

secondary bifurcation point q_s^{S} for different strut lengths where global buckling is critical. Note that for the perfect case strut, $q_s^{\mathrm{U}} \equiv q_s^{\mathrm{S}}$, as can be seen when comparing Figs. 12 and 10(a). Struts with an initial geometric global imperfection have a larger midspan

displacement at the secondary bifurcation point, compared to the perfect case. This can be attributed to the global imperfection having an effect on the global buckling mode, decreasing its load carrying capacity. However, a global initial imperfection would not have a large effect on the local buckling mode. This phenomenon is evidenced in the equilibrium paths plotted in Fig. 8, where the increase of q_{s0} has a significantly smaller effect on the equilibrium paths for the case where local buckling only is present. As a result, the distinct global and local buckling loads become further apart with an increasing global imperfection, for the case where global buckling dominates, thus the midspan displacement is more developed when the secondary instability is reached, resulting in a higher q_s^{S} value. An additional consequence of the global imperfection is that global buckling effectively remains dominant for shorter lengths of strut than L_c. The increase in the global buckling load for shorter struts is compensated by the decrease due to the global imperfection, causing global buckling to remain dominant for increasingly shorter lengths with a larger initial global imperfection. A similar trend would be expected for the variation of cross-section heights; it would also be expected that global buckling remains critical for deeper cross-sections as the size of global imperfections are increased.

6. Interactive buckling zones

Varying the length of the strut has a significant effect on the global buckling load, but a negligible effect on its local buckling load. In contrast, varying the cross-section height of the strut affects both the global and local buckling loads. Thus, owing to the changing buckling loads of the distinct modes, the strut is found to exhibit one of five different post-buckling behaviours that are hence summarized.

- For the ranges where $L < L_l$ or $h > h_l$, stable post-buckling is observed when the strut buckles in the local mode only. This is ultimately limited by yielding of the plates where the stresses are greatest.

- For the ranges $L_l < L < L_c$ or $h_c < h < h_l$, a stable post-buckling path is initially found where only the local mode is triggered, this is followed by an unstable path at a secondary instability, where the global buckling mode interacts with the local buckling mode. Failure is predicted to occur in the elastic range. However, in the parametric study of cross-section heights, this region can be further sub-divided into two further parts by the height h_s. In the range $h_c < h < h_s$, unstable post-buckling behaviour is observed following the secondary bifurcation point, whereas in the range $h_s < h < h_l$, this region of the post-buckling path is approximately neutral. There is no technical reason why a similar point could not be identified in the parametric study of strut lengths, but the exact location has not been found due to a less distinct change in post-buckling behaviour in that particular study.

- For $L = L_c$ or $h = h_c$, a highly unstable post-buckling path is found, where L_c and h_c are the critical length and height where global and local buckling are triggered simultaneously. Failure is likely to occur within the elastic range and a highly unstable post-buckling response, including a snap-back, would be expected.

- For the ranges $L_c < L < L_o$ or $h_o < h < h_c$, a neutrally stable post-buckling path is initially observed where only the global mode is triggered, followed by an unstable path after a secondary instability, where the local buckling mode interacts with the global buckling mode. Ultimately, the failure would be dominated by the elastic response.

- For $L > L_o$ or $h < h_o$, a neutrally stable post-buckling path is observed, when the strut buckles in the global mode only. This would ultimately be limited by either yielding of the extreme fibres or by serviceability criteria.

The lengths and heights found in the previous sections, where the perfect strut transitions between different post-buckling regions, are summarized in Table 2, along with their

	L_l	L_c	L_o		h_l	h_c	h_o
L [mm]	2646	3340	4950	h [mm]	84	116	145
λ_o	1.3047	1.6469	2.4408	λ_o	2.4408	1.6469	1.4166
λ_l	1.6915	1.6915	1.6915	λ_l	1.6276	1.7826	2.0396

Table 2: Summary of the transition lengths and heights that mark the regions of different post-buckling behaviours in the strut. The normalized global slenderness $\bar{\lambda}_o$ and local slenderness $\bar{\lambda}_l$ are also presented.

non-dimensional slendernesses. The normalized slendernesses $\bar{\lambda}$ are calculated using the definitions taken from Eurocode 3 [22] thus:

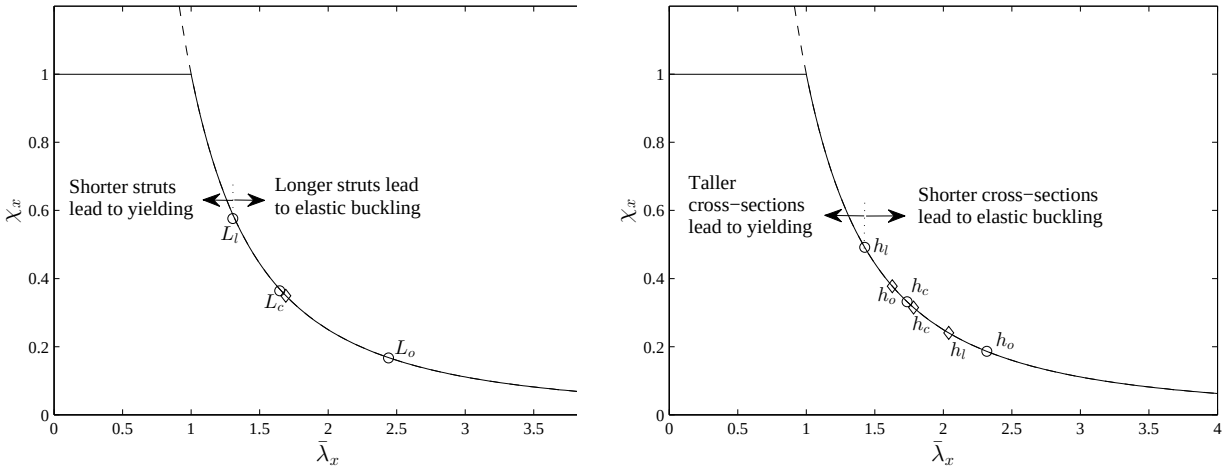
$$\bar{\lambda}_o = \sqrt{\frac{\sigma_{\mathrm{y}}}{\sigma_o^{\mathrm{C}}}}, \quad \bar{\lambda}_l = \sqrt{\frac{\sigma_{\mathrm{y}}}{\sigma_l^{\mathrm{C}}}}, \tag{21}$$

where subscripts 'o' and 'l' represent the global and local slendernesses respectively. The global buckling stress σ_o^{C} is calculated from the expression for P_o^{C} presented in Equation (20) and averaged over the cross-section. The local buckling stress σ_l^{C} is taken from the results of the linear eigenvalue analyses conducted in ABAQUS. Note that for the parametric study where L is varied, the global slenderness changes but the local slenderness remains constant. However, when the cross-section height h is varied, both global and local slendernesses change.

The normalized slendernesses given in Table 2 are plotted onto the compression strength curve taken from Eurocode 3, with subscript $x = \{o, l\}$ representing global or local slendernesses respectively. The parameter χ is essentially a buckling strength reduction factor with values below unity indicating that the strut has an ultimate stress that is less than the material yield stress, due to the effects of elastic instability thus:

$$\chi_o = \frac{\sigma_o^{\mathrm{C}}}{\sigma_{\mathrm{y}}}, \quad \chi_l = \frac{\sigma_l^{\mathrm{C}}}{\sigma_{\mathrm{y}}}. \tag{22}$$

The idealized compression strength curves indicate that when the strut slenderness is such that $\bar{\lambda}_x < 1$, it will fail primarily due to material yielding, and for slendernesses of $\bar{\lambda}_x > 1$, the strut will fail primarily due to elastic buckling. Figure 13(a) shows the



(a) (b)

Figure 13: The idealized compression strength curves with circles representing the global slenderness $\bar{\lambda}_o$ and the diamonds representing the local slenderness $\bar{\lambda}_l$ for the parametric study of (a) strut lengths and (b) cross-section heights. The strut length and cross-section heights for each point is labelled accordingly. The arrows indicate the slenderness marking the boundary where elastic buckling or yielding govern the ultimate response.

global and local slenderness from the parametric study of strut lengths and in Fig. 13(b) from the corresponding study of cross-section heights. It can be observed that for the critical length L_c and height h_c, where interactive behaviour is most severe, the global and local slendernesses are extremely close with an almost identical buckling stress, as found earlier.

It can also be seen from the graphs for all struts that elastic buckling appears to dominate the post-buckling behaviour. However, since a first yield criterion is used to determine the transition length L_l and height h_l, it can be seen that yielding actually occurs for a larger slenderness than that determined simply by the idealized compression strength curves. The idealized compression strength curves are plotted based on the assumption that the load is evenly distributed throughout the cross-section and develops at the same rate throughout the strut. However in reality, as soon as components of the strut exhibit buckling deformations, the load becomes unevenly distributed causing certain areas of the strut to experience much higher stresses. Therefore, specific areas of the strut would reach the yield stress and limit the load carrying capacity. For both parametric studies, it is the global slenderness that determines the lower limit where yielding dominates the post-buckling behaviour. Note that throughout the parametric studies, a high material yield stress has been considered, but if a more standard grade of steel is considered with a much lower yield stress (for example $\sigma_y = 460\,\mathrm{N/mm^2}$), material yield would occur for a higher

slenderness than has been determined currently and may destabilize the already unstable interactive response [25]. Moreover, if a material with a sufficiently low yield stress is considered, the material yield limit could be reached before any interactive post-buckling behaviour is observed. This is of course common in the behaviour of compact hot-rolled steel components where local buckling does not usually occur within the elastic range [26].

7. Concluding remarks

A set of parametric studies has been presented for a range of example strut properties to investigate the effects of changing the length and cross-section height of an I-section strut. The analytical model, developed in [14] and summarized in §2.2, was used to conduct the parametric study for the struts where global buckling is critical. The FE model, developed in the software ABAQUS, was used to conduct the parametric study for struts where local buckling is critical. A serviceability criterion, based on limiting deflections, is primarily used to define the interactive buckling region, but an additional strain based criterion is also introduced, which is particularly important where local buckling is critical, since the load carrying capacities for these geometries are much more likely to be affected by the effects of excessive strains and hence material failure. The parametric study reveals the strut geometries that define the different regions of post-buckling behaviour.

The global and local slendernesses of the struts at the transition lengths and cross-section heights are also analysed. It is found that for both studies, the global and local slenderness of the strut at L_c and h_c are very similar, with almost identical buckling stresses. In both studies, it is the global slenderness that determines the lower limit where yielding begins to dominate the ultimate behaviour.

It may be concluded that the cases where local and global buckling are triggered simultaneously should be treated with caution in design due to the highly unstable nature of the post-buckling response. The effects of the presence of an initial geometric out-of-straightness in the strut were also analysed in the parametric study of the strut length, and it was determined that the ranges that experience interactive buckling ($i.e.\, L_l < L < L_o$) are highly sensitive to initial imperfections. This further emphasizes the potential problems of designing components such that global and local buckling loads lie close together. The effect of the initial global imperfection is anticipated to have an identical qualitative effect on the parametric study of cross-section heights where $h_o < h < h_l$.

The current study and methodology can be extended to investigate the effects of changing other geometries affecting the local slenderness of the strut (for example, the plate thickness), as well as the effects of initial geometric local imperfections. However, other geometric variations of the strut can be analysed by considering the normalized slendernesses for both global and local buckling. In this way, the current analysis can indicate whether the limiting strength of the material will be observed in the strut. This would enable the maximization of the true geometric and material strengths, leading to inherently more efficient designs.

Acknowledgement

Financial support for the lead author was provided by the UK Engineering and Physical Sciences Research Council under the Doctoral Training Grant scheme.

References

[1] J. M. T. Thompson, G. W. Hunt, A general theory of elastic stability, John Wiley and Sons Ltd, London, UK, 1973.

[2] W. T. Koiter, M. Pignataro, A general theory for the interaction between local and overall buckling of stiffened panels, Tech. rep., WTHD Report 91, Delft, The Netherlands (1976).

[3] J. M. T. Thompson, G. W. Hunt, Elastic instability phenomena, John Wiley and Sons Ltd, Chichester, UK, 1984.

[4] V. Gioncu, General theory of coupled instabilities, Thin-Walled Structures 19 (2–4) (1994) 81–127.

[5] A. van der Neut, The interaction of local buckling and column failure of thin-walled compression members, in: M. Hetenyi, W. G. Vincenti (Eds.), Proceedings of the 12th International Congress of Applied Mechanics, 1969, pp. 389–399.

[6] J. Becque, K. J. R. Rasmussen, Experimental investigation of the interaction of local and overall buckling of stainless steel I-columns, ASCE J. Struct. Eng 135 (11) (2009) 1340–1348.

[7] M. A. Wadee, L. Gardner, Cellular buckling from mode interaction in I-beams under uniform bending, Proc. R. Soc. A 468 (2137) (2012) 245–268.

[8] M. A. Wadee, M. Farsi, Cellular buckling in stiffened plates, Proc. R. Soc. A 470 (2168) (2014) 20140094.

[9] M. A. Wadee, L. Bai, Cellular buckling in I-section struts, Thin-Walled Struct. 81 (2014) 89–100.

[10] M. A. Wadee, M. Farsi, Imperfection sensitivity and geometric effects in stiffened plates susceptible to cellular buckling, Structures 3 (2015) 172–186.

[11] A. D. Martins, D. Camotim, P. B. Dinis, B. Young, Local–distortional interaction in cold-formed steel columns: Mechanics, testing, numerical simulation and design, Structures 4 (2015) 38–57.

[12] L. Bai, M. A. Wadee, Slenderness effects in thin-walled I-section struts susceptible to local-global mode interaction, Engineering Structures 124 (2016) 128–141.

[13] E. L. Liu, M. A. Wadee, Interactively induced localization in thin-walled I-section struts buckling about the strong axis, Structures 4 (2015) 13–26.

[14] E. L. Liu, M. A. Wadee, Mode interaction in perfect and imperfect thin-walled I-section struts susceptible to global buckling about the strong axis, Thin-Walled Struct. 106 (2016) 228–243.

[15] M. A. Wadee, S. Yiatros, M. Theofanous, Comparative studies of localized buckling in sandwich struts with different core bending models, Int. J. Non-Linear Mech. 45 (2) (2010) 111–120.

[16] S. P. Timoshenko, S. Woinowsky-Krieger, Theory of plates and shells, McGraw–Hill College, New York, USA, 1959.

[17] G. W. Hunt, M. A. Wadee, Localization and mode interaction in sandwich structures, Proc. R. Soc. A 454 (1972) (1998) 1197–1216.

[18] ABAQUS, Version 6.14, Dassault Systèmes, Providence RI, USA, 2014.

[19] M. A. Wadee, M. Farsi, Local-global mode interaction in stringer-stiffened plates, Thin-Walled Struct. 85 (2014) 419–430.

[20] J. Becque, K. J. R. Rasmussen, Numerical investigation of the interaction of local and overall buckling of stainless steel I-columns, ASCE J. Struct. Eng. 135 (11) (2009) 1340–1348.

[21] E. Riks, An incremental approach to the solution of snapping and buckling problems, Int. J. Solids Struct. 15 (7) (1979) 529–551.

[22] EN1993-1-1, BSI, Part 1-1: General rules and rules for buildings (2005).

[23] EN10210, BSI, British Standard: Hot finished structural hollow sections of non-alloy and fine grain steels Part 2: Tolerances, dimensions and sectional properties (2006).

[24] H. P. Günther, Use and Application of High-Performance Steels for Steel Structures (SED 8), IABSE, Switzerland, 2005.

[25] J. Becque, Local–overall interaction buckling of inelastic columns: A numerical study of the inelastic Van der Neut column, Thin-Walled Struct. 81 (2014) 101–107.

[26] N. S. Trahair, M. A. Bradford, D. Nethercot, L. Gardner, The behaviour and design of steel structures to EC3, CRC Press, New York, USA, 2007.